Simulation of high-power pulse generation due to modelocking in long multisection lasers

K.-H. Hasler, A. Klehr, H. Wenzel and G. Erbert

Abstract: The dynamic behaviour of long monolithic modelocked lasers for the emission wavelength 1.06 μm containing an active gain section and a passive cavity section was simulated. Numerical tools have been used to solve the travelling wave and carrier rate equations taking into account the effect of gain dispersion. Different configurations and arrangements including an absorber section and a section with a DBR were studied and compared. Best pulses are achieved with a configuration having a saturable-absorber section at the front facet. Peak powers of more than 5 W, pulse energies greater then 15 pJ and time-bandwidth products less than 0.5 are obtained by optimising the resonator configuration.

1 Introduction

High-power optical pulses with a small spectral width and with repetition rates of a few GHz are required for several applications, such as free space optical communication or frequency conversion. Although high-power pulses can be generated by solid state lasers, semiconductor lasers offer the advantages of small size, high efficiency, excellent reliability and ease of handling. Typically, optical pulses can be generated by gain switching, active or passive Q-switching or modelocking. Gain switching can be achieved by a direct modulation of the driving current of an active section. Q-switching is related to a change of the modal absorption of a saturable absorber introduced some where into the cavity (absorptive type) [1] or to a change of the wavelength-dependent feedback of a DBR (dispersive type) [2]. In [3] we have used a DBR laser with an emission wavelength of 1.06 μm, containing gain, absorber and Bragg-grating sections to generate high-power pulses by absorptive Q-switching. Although absorptive Q-switching yields high peak-powers, the time-bandwidth products exceed the transform limit considerably and is typically around 2 [3].

Modelocking is a way of short pulse generation in which an optical pulse is repetitively reshaped as it circulates in the laser cavity. To achieve short optical pulses from a laser, the different longitudinal modes of the laser cavity must have a fixed phase relationship such that at periodic intervals all the modes are approximately in phase. In the modelocking mode of operation a balance exists between mechanisms that tend to shorten and to widen the pulses. In contrast to Q-switching the repetition rate of modelocked pulses is only determined by their round-trip time in the laser cavity. The quality of short optical pulses is characterised by their time-bandwidth product (TBP), which is the product of the temporal width and the spectral width of a pulse. It is always larger than the so called transform or Fourier limit.

Modelocking techniques can be classified as active, passive, or hybrid. Overviews for modelocked semiconductor lasers are given in [4–7]. Active modelocking employs modulation of the gain to shape the pulse. A suitable saturable absorber is a key element for passive modelocking. The laser is driven by a constant current and no external modulation is used. Hybrid modelocked lasers can combine the short, single-pulse capabilities of passive modelocked lasers with the small timing jitter and stable operation of active modelocked lasers. Modelocking can be realised in external cavities or in monolithic cavities [4, 6]. For repetition frequencies up to several GHz external cavities are used owing to the round-trip time needed [4–6]. Monolithic-cavity modelocked laser structures are very compact and do not exhibit the mechanical instabilities associated with optical elements in an external cavity. Typically they can generate pulses with repetition frequencies of several tens of GHz [8]. Despite the need of long cavities, monolithic modelocked lasers for smaller repetition frequencies were investigated, too [9–12]. Although small pulse widths and low time-bandwidth products were obtained, the pulse energies remained far below 1 pJ.

In this paper, different types of long monolithic multisection lasers are analysed numerically. The aim is to find a configuration which delivers optical pulses with repetition rates in the GHz range with peak powers of several Watts and time-bandwidth products near the transform limit. The multisection lasers under investigation consist at least of an active gain section and a passive cavity section. The total resonator length is about 1 cm. The impact of absorber and distributed DBR sections are studied and compared. In our structures the active layer extends over all sections, so an unpumped section can act as saturable absorber. The absorption can be strongly increased by a selective heating of this section and can be decreased by injecting of a small current pulse through the p-n junction. This offers the possibility of hybrid modelocking. Hybrid modelocking means in this paper that the gain section is pumped with a large constant current whereas relatively small current pulses with a repetition rate determined by the photon round-trip time are injected into the saturable absorber. The section containing the DBR determines the centre

© IEE, 2005

IEE Proceedings online no. 20045038

doi: 10.1049/ip-opt:20045038

Paper first received 27th July and in revised form 13th December 2004

The authors are with the Ferdinand-Braun-Institut für Höchstfrequenztechnik, Gustav-Kirchhoff-Straße 4, 12489 Berlin, Germany

E-mail: hasler@fbh-berlin.de

wavelength of the pulses and can improve the modelocking behaviour and pulse properties, if properly designed [4, 13, 14].

Numerical simulations of modelocking in semiconductor lasers are mostly performed with a mixed-frequency time-domain approach, for instance numerical lumped–element models [15], fully-distributed time-domain models [4, 16, 17] and the transmission-line laser model [18, 19]. For a recent review we refer to [7]. Sometimes purely frequency–domain approaches are used, see [20, 21]. For our investigations we use the mixed-frequency time-domain simulation program LDSL [22] which solves numerically the travelling wave equations and the carrier- density rate equation [23–25] taking into account gain dispersion [26, 27]. It allows us to calculate accurately the spatio-temporal behaviour and the optical spectrum of semiconductor lasers consisting of an arbitrary number of different sections.

The paper is organised as follows. In Section 2 the basic structure and the numerical model used are described. In Section 3 the results of a comparative study of different configurations and arrangements are presented, including a detailed investigation of an optimised structure. Finally, the main results are summarised.

2 Basic structure and numerical model

The basic laser structure underlying the simulation can be found in [3, 28–30]. A schematic view of the multisection laser is shown in Fig. 1. Aiming to a repetition frequency of about 4 GHz, the total cavity length has to be around 1 cm. Typical lengths used in the simulations are $L_G = 500$–1000 μm for the gain section, $L_A = 200\,\mu m$ for the absorber section, $L_{Cav} = 8300$–$9300\,\mu m$ for the passive cavity section and $L_{DBR} = 100$–$500\,\mu m$ for the DBR section. The active layer consists of a compressively strained InGaAs single quantum well (QW) which extends over all sections. The emission wavelength is 1.06 μm.

The absorber effect is caused by the interband absorption of the QW. It can be enhanced by selective heating of the corresponding section, using a current flow along the ridge [3], see also Fig. 1. The action of the selective heating of the absorber section is modelled by an appropriate choice of the gain parameters transparency density N_{tr} and modal differential gain g_{diff} as described in [3]. It is known [31], that the differential gain increases if the difference between photon and band gap energies is enlarged. Additionally, the transparency density increases, too. The actual dependencies of these gain parameters on the heating currents is difficult to calculate, because one has to determine the distributions of the temperature, the electrostatic potential in

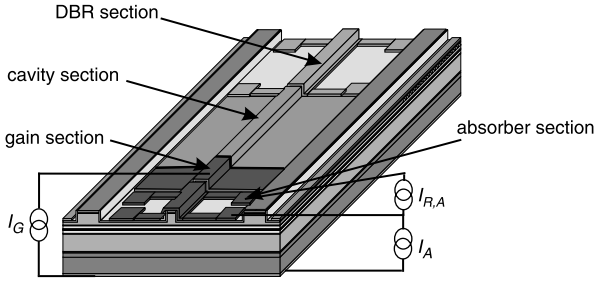

Fig. 1 *Schematic view of multisection laser emitting at $\lambda = 1060$ nm containing absorber and Bragg-grating sections*

The epitaxial layers including the active InGaAs QW extend over all sections. Selective heating of the absorber section using a current flow $I_{R,A}$ along the ridge

Table 1: Selected parameters used in the simulations

Parameter	Symbol	Values
Length of gain section	L_G	500–1500 μm
Length of absorber section	L_A	100–300 μm
Length of DBR section	L_{DBR}	100–500 μm
Length of the cavity	L_{Cav}	7700–9500 μm
Stripe width	W	5 μm
QW thickness	D	8 nm
Coupling coefficient	κ	40 cm^{-1}
Non-radiative recombination lifetime	τ_{nr}	10 ns
Radiative recombination coefficient	B	2×10^{-10} cm^3 s^{-1}
Auger recombination coefficient	C	0
Differential gain	g_{diff}	24×10^{-18} cm^2
Differential gain of absorber section	g_{diff}	100×10^{-18} cm^2
Carrier density for transparency	N_{tr}	0.8×10^{18} cm^{-3}
Carrier density for transparency of absorber section	N_{tr}	5–24×10^{18} cm^{-3}
Nonlinear gain compression factor	ε	0.3×10^{-18} cm^3
Henry's α-factor	α_H	−1.3
Group index	$n_g = c/v_g$	4.0
Internal optical losses	α	5 cm^{-1}

dependence on the excess carrier densities within the device, coupled to a microscopic gain model including many-body corrections. Therefore, we used N_{tr} and g_{diff} of the absorber section merely as fit parameters. The absorption can be rapidly temporally decreased by injecting a current pulse through the p-n junction or by generating excess carriers owing to the absorption of photons. It should be mentioned, that in the present study the same recombination parameters are used in the absorber as in the other sections (see Table 1).

The numerical simulations are performed using the LDSL tool [22, 32]. In the following, the basic equations are briefly described. A detailed description can be found in [23–25] and [26, 27]. The optical field within the laser assumed to be TE-like polarised is decomposed into two counter-propagating waves along the longitudinal axis z. The slowly varying amplitudes $\Psi^{\pm}(z,t)$ of the optical fields obey the well-known travelling wave equations (TWEs) [33]. In order to model gain dispersion, the TWEs are coupled with polarisation functions $p^{\pm}$, which satisfy the linear ordinary differential equation [26, 27]

$$-\mathrm{i}\frac{dp^{\pm}}{dt} = (\Omega_r + \mathrm{i}\Gamma)p^{\pm} + \Gamma\Psi^{\pm} \tag{1}$$

via the additional term

$$\Delta\beta\Psi^{\pm} = \frac{G_r}{2}p^{\pm} - i\frac{G_r}{2}\Psi^{\pm} \tag{2}$$

This model for the polarisation originates from a Lorentzian approximation of the gain spectrum. The parameters in (1), (2) and of the Lorentzian, respectively were fitted to microscopic gain calculations with the following result:

$$G_r = 20\,\mathrm{cm}^{-1}, \quad \Omega_r = -\frac{\omega_0^2}{2\pi c}\cdot 2\,\mathrm{nm}, \quad \Gamma = \frac{\omega_0^2}{2\pi c}\cdot 15\,\mathrm{nm}.$$

The carrier density dependence of the gain peak is taken linear expressed by the differential gain g_{diff} and transparency carrier density N_{tr}, which were chosen differently in the absorber and the other sections. It should be mentioned, that (1) leads also to an additional index dispersion.

The travelling wave equations are coupled via the optical power $P = |\Psi^+|^2 + |\Psi^-|^2$ to the carrier-density rate equation [26, 27, 32, 33] for every section. The carrier density depends on the longitudinal axis z, because the injected current may differ from section to section (this leads to different, but constant carrier densities in every section) and because the local optical power depends on z via the TWEs (this leads to a continuously varying carrier density in every section).

The ratio of the discretisation steps in space and time is given by the group velocity. We used an equidistant longitudinal discretisation $\Delta z = 10\,\mathrm{nm}$ yielding a temporal discretisation $\Delta t = 133.3\,\mathrm{fs}$ which is a compromise between sufficient accuracy and moderate simulation time. Note that the photon round-trip time is about 260 ps for the 1 cm-long devices. The basic parameters used in the simulations are listed in Table 1. For the calculation of the optical spectra via a Fourier transformation we used a time interval of 546 ps with 4096 time points which results in a frequency resolution of 1.83 GHz (wavelength resolution 0.0061 nm). In order to minimise finite-time interval effects on the spectrum, the data are multiplied with a Hamming-window function [22, 32].

The gain parameters were obtained from a microscopic gain model, based on the bandstructure calculated with an eight-band $\mathbf{k}\cdot\mathbf{p}$ model taking into account all possible transitions as outlined in [34]. Many-body effects were taken into account by phenomenological corrections for the gain spectral broadening and for the band-gap renormalisation. The parameters entering the model were compiled from different sources in the literature and are similar to those given in [35]. The Henry factor α_H was also estimated from the microscopic calculations. Due to the fact, that for our highly-strained InGaAs QW the magnitude of α_H is rather small, its value has only a minor influence on the results. Moreover, the dependence of the refractive index change on the carrier density is only very roughly described by the product of α_H and the gain [34]. Hence, we decided to use the same value for α_H in all sections.

3 Results

3.1 Comparative study of different structures

We investigate various structures for active, passive and hybride modelocking with a Fabry–Perot resonator in addition to an additional integrated DBR. For a schematic view of the multisection structure containing absorber and Bragg-grating sections see Fig. 1. The analysed structures are listed and described schematically in Table 2. The obtained results are summarised in Table 3. The chosen currents I_G through the gain section given in column two were kept constant for comparable structures. Other values for I_G yielded the same performance ranking of the different structures. The front facet where the pulses are emitted is located at the left side.

First we consider active modelocking in a simple two-section structure containing only a directly modulated gain section and the cavity section (structure 0 in Table 2). The total length of the monolithic structure is 1 cm and the length of the gain section is 500 µm. The reflectivities of the front and rear facets are 0.05 and 0.8, respectively. Here, and for all other cases, internal reflectivities between the sections are assumed to vanish. The modulation frequency of the gain-section current determined by the photon round-trip time is 3750 MHz. The gain section is additionally pumped with a constant current of $I_G = 10\,\mathrm{mA}$ for a maximum pulse power. The passive section is also pumped with a constant current until near the transparency (for lowering the optical losses) which is a critical parameter. The locking time is around 30 ns (then a stationary state is reached) and the locking range (maximum difference between modulation frequency and round-trip frequency) is around 10 MHz. Figure 2 shows a single modelocked pulse and the corresponding optical spectrum for sinusoidal shaped gain-current pulses with an amplitude of 75 mA and a length of 133 ps. The pulse width (FWHM) is 3.7 ps and the time-bandwidth product is around 0.89. The pulse energy is around 1.2 pJ. In the simulations irregular fluctuations of the peak power of about 20% in the range of some nanoseconds can be observed.

To achieve smaller spectral widths Δf of the pulses a DBR is added (structure 1A and 1B in Table 2). Then the gain section can be arranged also in the middle (structure 1B). The length of the DBR section is 500 µm and the coupling coefficient is $40\,\mathrm{cm}^{-1}$, which yields a reflectivity of around 93%. The reflectivity of the front facet is 0.05 and the reflectivity of the rear facet of the DBR section is set to zero. The modulation frequency is slightly increased because of the shorter round-trip time (length of the current pulses now around 127 ps). It is advantageous for a maximum pulse power to pump the DBR section with a small constant current to decrease the absorption there. Generally, the DBR stabilises the pulse amplitudes, so that the peak power fluctuations vanish. The locking time is strongly decreased and is now less then 10 ns and the locking range is increased up to 20 MHz. The numerical experiments show that the reflectivity at the facet of DBR section should be generally less then 10^{-2} for a stable modelocking at the Bragg wavelength. In order to avoid the appearance of artefacts at the trailing flanks of the pulses the facet reflectivity at the DBR section should be, as a maximum, 10^{-4}. This finding is in agreement with the results of other authors [36]. The magnitude of the coupling coefficient of the DBR on the modelocking behaviour is not critical. Figure 3 shows modelocked pulses and Fig. 4 the corresponding optical spectra for structures 1A and 1B. Structure 1A, where the gain section is positioned at the front side, yields the higher peak power. As expected, the spectral width is decreased, but the pulse width is increased so that the time-bandwidth product is in the same range as for structure 0. The pulse energy is decreased (around 0.6 pJ) for structure 1A and is strongly decreased (around 0.1 pJ) for structure 1B caused by the absorption in the cavity section. If we try to decrease the losses by strongly increasing the current in the cavity section then the modelocking is destroyed by light generation there. Therefore structures where the gain section is arranged after the passive section are not further investigated.

We note that one advantage of using a DBR is that the lasing wavelength is fixed by the DBR. By further numerical experiments we found that a stable modelocking occurs only if the difference between the Bragg wavelength and the wavelength of the gain maximum is smaller then 3.5 nm for our gain dispersion parameters. Otherwise the modelocking at the Bragg wavelength is destroyed. The DBR reduces the number of simultaneously lasing longitudinal modes building up the pulse owing to the finite bandwidth of the reflectivity spectrum.

Table 2: Overview of the different configurations investigated

Structure	Arrangement of the sections	Typical section lengths (μm)	Types of modelocking
0	gain/cavity	500/9500	active
1A	gain/cavity/DBR	500/9000/500	active
1B	cavity/gain/DBR	9000/500/500	active
2A	gain/absorber/cavity	500/200/9300	hybrid
2B	absorber/gain/cavity	200/500/9300	hybrid + passive
2C	gain/cavity/absorber	500/9300/200	hybrid
3A	gain/absorber/cavity/DBR	500/200/8800/500	hybrid
3B	absorber/gain/cavity/DBR	200/500/8800/500	hybrid + passive
3B optim.	absorber/gain/cavity/DBR	200/1000/8300/100	hybrid + passive
3C	gain/cavity/absorber/DBR	500/8800/200/500	hybrid

Table 3: Performance of the different configurations investigated

Structure	I_G (mA)	Peak power (mW)	Pulse energy (pJ)	FWHM (ps)	Δf (nm)	TBP
0	10 + 75 sin .	298	1.22	3.7	0.8	0.89
1A	10 + 75 sin .	68.2	0.61	8.3	0.4	1.0
1B	10 + 75 sin .	11.3	0.12	9.9	0.3	0.89
2A	50	687	2.4	3.1	0.6	0.56
2B	50	718	3.3	3.9	0.7	0.81
2C	50	494	2.6	4.7	0.8	1.13
3A	50	167	1.3	7.2	0.6	1.3
3B	50	231	2.1	8.5	0.4	1.0
3C	50	214	1.7	7.5	0.4	0.9
3B optim.	100	1735	6.3	2.9	0.6	0.52
3B optim.	200	3781	12.6	2.8	0.55	0.46
3B optim.	300	5223	16.2	2.5	0.55	0.41

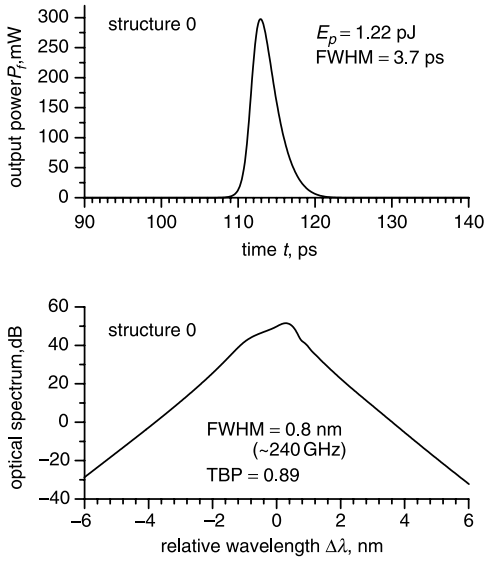

Fig. 2 *Structure **0**, single actively modelocked pulse (top) and optical spectrum (bottom) for sinusoidal shaped gain-current pulses with amplitude $\Delta I_G = 75$ mA and repetition frequency $f = 3750$ MHz (length 133 ps)*

$L_G = 500\,\mu m$, $I_G = 10$ mA, $L_{Cav} = 9500\,\mu m$, $I_{Cav} = 20$ mA, $R_f = 0.05$, $R_r = 0.8$

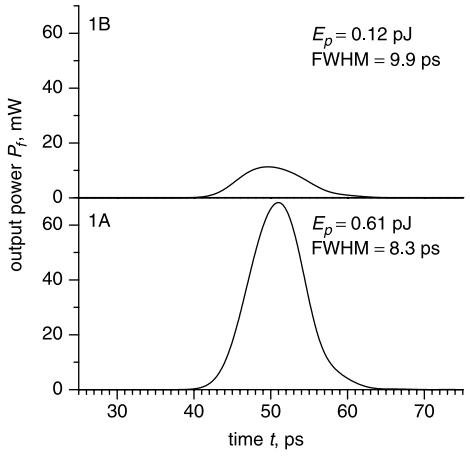

Fig. 3 *Structures 1A and 1B, actively modelocked pulses for sinusoidal shaped gain-current pulses with amplitude $\Delta I_G = 75$ mA and repetition frequency $f = 3920$ MHz (length 127.5 ps)*

$L_G = 500\,\mu m$, $I_G = 10$ mA, $I_{Cav} = 20$ mA, $I_{DBR} = 1.32$ mA, $L_{Cav} = 9000\,\mu m$, $L_{DBR} = 500\,\mu m$, $R_f = 0.05$, $R_r = 0$

Higher pulse energies can be obtained by adding a saturable absorber for hybrid and passive modelocking. There exist several possible arrangements of the different sections, but only three of them promise good results (because of losses in the cavity section) and were investigated in more detail. The investigated structures with absorber section, but without DBR section, are denoted by 2A–C and are described in Table 2. The length of the absorber section in the simulations is 200 μm. The reflectivities of the front and rear facets are 0.05 and 0.8, respectively.

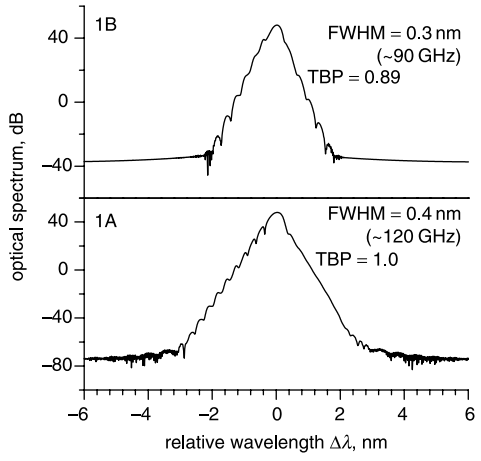

Fig. 4 *Structures 1A and 1B, optical spectra of pulses shown in Fig. 3*

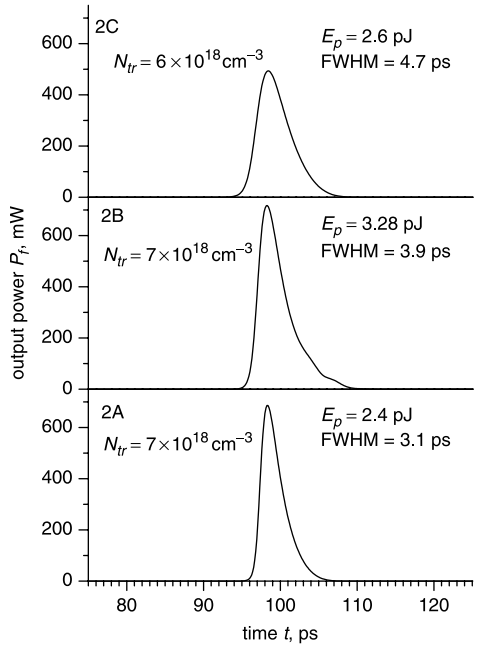

Fig. 5 *Structures 2A, 2B and 2C, optical pulses due to hybrid mode locking for sinusoidal shaped absorber-current pulses with amplitude $\Delta I_A = 30$ mA and repetition frequency 3750 MHz*

$I_G = 50$ mA, $I_{Cav} = 25$ mA, $L_G = 500$ µm, $L_{Cav} = 9300$ µm, $L_A = 200$ µm, $R_f = 0.05$, $R_r = 0.8$. The transparency density in the absorber section is indicated

Figure 5 shows modelocked pulses for the structures 2A–C for sinusoidal shaped absorber-current pulses with an amplitude ΔI_A of 30 mA and a length of 133 ps. The constant gain-section current I_G is 50 mA and the current injected into the cavity section I_{Cav} is 25 mA. The advantages compared to the corresponding structure without saturable absorber are the considerably increased peak powers and the smaller pulse widths hence smaller time-bandwidth products. However, fluctuations of the peak power are observed, too. Figure 6 shows the corresponding spectra with spectral widths (FWHM) around 0.7 nm. The locking times and locking ranges are nearly the same as for structures without saturable absorber. The highest pulse energies are obtained for structure 2B (absorber/gain/cavity) and the smallest time-bandwidth products are obtained for structure 2A (gain/absorber/cavity), see also Table 3.

If a DBR section is included at the rear facet (structures 3A, 3B and 3C in Table 2) the amplitudes of the

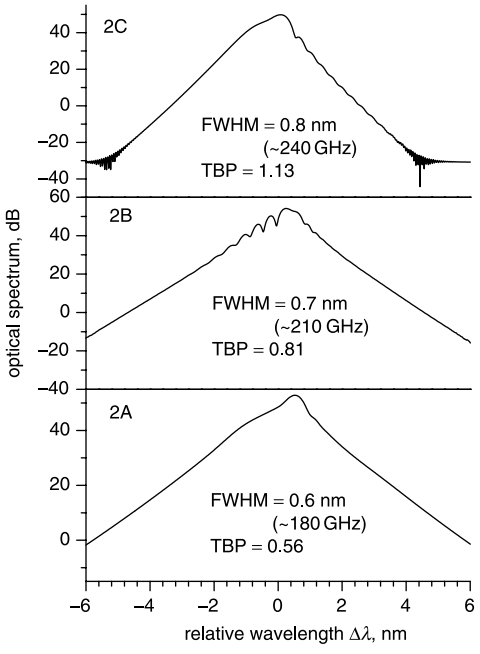

Fig. 6 *Structures 2A, 2B and 2C, optical spectra of pulses shown in Fig. 5*

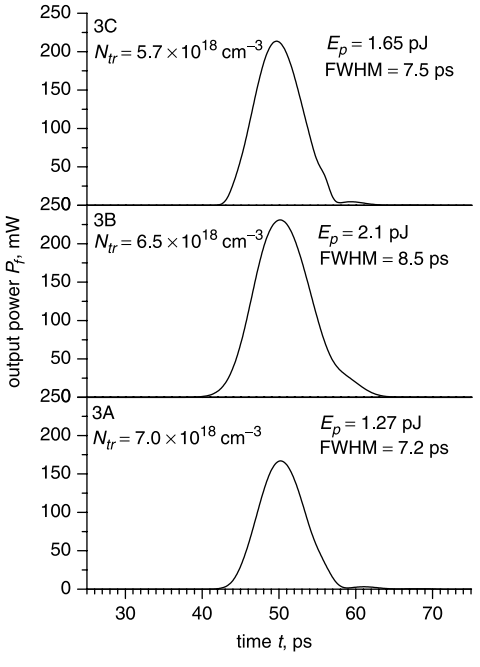

Fig. 7 *Structures 3A, 3B and 3C, optical pulses due to hybrid mode locking for sinusoidal shaped absorber-current pulses with amplitude $\Delta I_A = 30$ mA and repetition frequency 3927 MHz (length 127.3 ps)*

$I_G = 50$ mA, $I_{Cav} = 25$ mA, $I_{DBR} = 1.0$ mA, $L_G = 500$ µm, $L_{Cav} = 8800$ µm, $L_A = 200$ µm, $L_{DBR} = 500$ µm, $R_f = 0.05$, $R_r = 0$. The transparency density in the absorber section is indicated

mode-locked pulses are again stabilised so that the peak-power fluctuations vanish. The pulse widths are increased whereas the peak powers are strongly decreased as can be seen from Fig. 7 and Table 3. The pulse energies also become smaller. Figure 8 shows the corresponding spectra with spectral widths of around 0.5 nm. The length of the DBR section is 500 µm whereas the magnitude of the injected currents are the same as before. The spectral widths of the pulses of structures 3B and 3C are smaller than for the corresponding structures 2B and 2C without DBR. The shape of the spectrum of structure 3B differs considerable

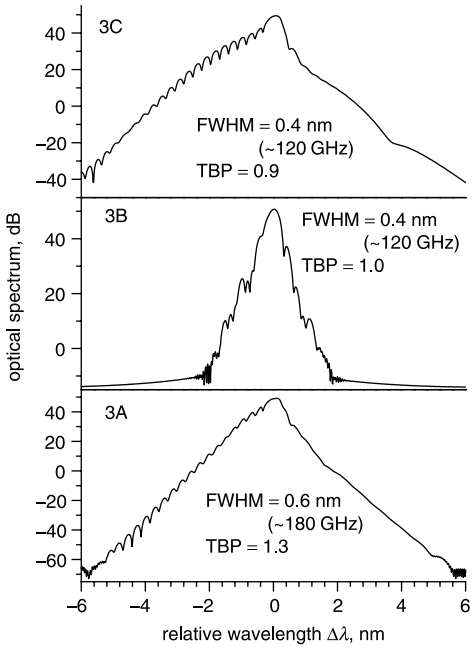

Fig. 8 *Structures 3A, 3B and 3C, optical spectra of pulses shown in Fig. 7*

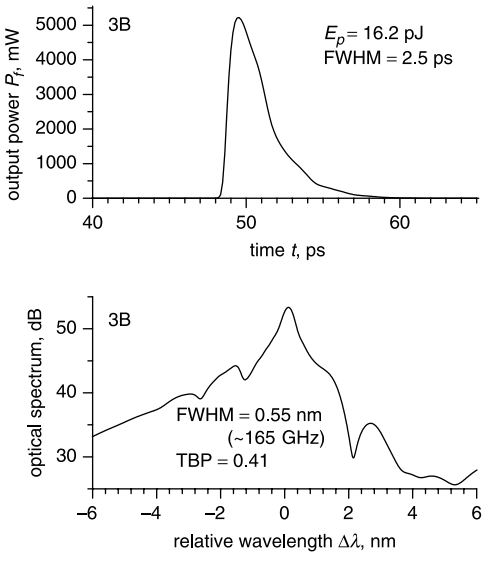

Fig. 9 *Optimised structure 3B, high-power optical pulse (top) and optical spectrum (bottom) due to passive modelocking*

$I_{Cav} = 50$ mA, $I_{DBR} = 0$, $L_G = 1000$ µm, $I_G = 300$ mA, $L_{Cav} = 8300$ µm, $L_A = 200$ µm, $L_{DBR} = 100$ µm, $\kappa = 30\,\text{cm}^{-1}$, $R_f = 0.05$, $R_r = 10^{-4}$. Absorber section: $N_{tr} = 23 \times 10^{18}\,\text{cm}^{-3}$

from the other ones. The time-bandwidth product is in the same range for structures 3B and 3C and larger for structure 3A. The advantages compared to the corresponding structures without saturable absorber are again considerably increased pulse powers. The pulse widths and the time-bandwidth products are nearly the same. Structure 3A yields a lower peak power. The best results are obtained for structure 3B. For both structures 3A and 3C we observe artifacts at the trailing edges of the pulses, they vanish for shorter Bragg-reflector lengths. Note, that for both structures A and C stable modelocking was achieved only at low gain-section currents less than 100 mA. This is also valid for the corresponding structures without DBR.

3.2 Detailed investigation of structure 3B

The structure 3B (absorber/gain/cavity/DBR) containing a saturable absorber as the section closest to the emission mirror and a DBR as the last section was investigated in more detail, because it seems most promising for generation of pulses with very high peak power. Passive modelocking is also possible for this structure, but then more jitter is expected. The higher the gain current and hence the pulse peak power, the more the carrier generation owing to interband-absorption of photons dominates over the carrier generation due to the external absorber current. Hence, for sufficiently high gain-section currents the current modulation of the absorber section triggers only the process. Also at high gain-section currents a strong longitudinal hole burning was found in the gain section.

By numerical experiments we found that the length L_{DBR} of the DBR section must be chosen carefully, especially at higher gain-section currents. The optimal length of the DBR section lies in the range between 100–200 µm for the coupling coefficient of 20–40 cm^{-1} assumed here and is a compromise between small pulse width and time-bandwidth product and large pulse energy. Figure 9 shows an example for passive modelocking with an optimised structure for a gain-section current of 300 mA and a gain-section length of 1000 µm. The DBR length is only 100 µm and the coupling coefficient is 30 cm^{-1}, which yields a reflectivity of around 8.5%. We obtained pulse powers of more than 5 W and pulse energies of more than 15 pJ, see also Table 3. This corresponds to an averaged power of more then 60 mW. The pulse width is around 2.5 ps and the spectral width is around 0.5 nm. We obtained a time-bandwidth product of 0.41. This is very close to the transform limit of 0.441 for a Gaussian pulse [37] and 0.315 for a sech^2 pulse shape [8]. For comparison the pulse parameters at gain-section currents of 100 and 200 mA, respectively, are also listed in Table 3. Note that for higher gain-section currents the pulse width is decreasing. For gain-section currents of more than 350 mA no stable modelocking at the round-trip frequency can be obtained. But stable modelocking at the second (or even third) harmonic can be observed if the gain-section current is increased more and more.

Figures 10 and 11 depict the dependence of the pulse energy on the gain–sectional length and current. A further increase of the gain-section length to values larger than 1000 µm does not lead to a further increase of the pulse energies. The same holds for an increase of I_G above 300 mA. This is caused by the increased amplified spontaneous emission before the pulse, compare Fig. 12*a*. Generally, at higher gain-section currents the pulses become more asymmetric with a large trailing edge. Figure 13 shows the starting of hybrid modelocking for the same optimised

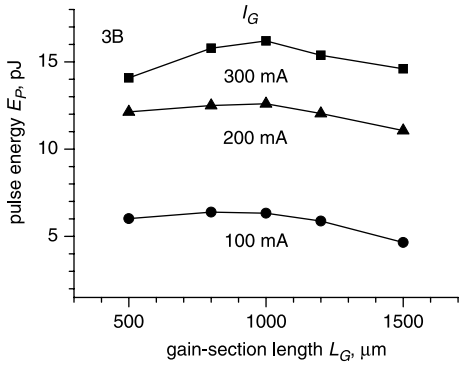

Fig. 10 *Structure 3B, pulse energy dependence on length of gain section for different currents through this section*

Absorber section: $N_{tr} = 10$–$25 \times 10^{18}\,\text{cm}^{-3}$. Other parameters same as Fig. 9

structure 3B. The amplitude ΔI_A of the absorber-current pulses is also only 30 mA. Nearly the same picture is obtained for passive modelocking. Generally, at lower gain currents smaller pulse energies were obtained as for hybrid modelocking whereas at higher gain currents nearly the same pulses for hybrid and passive modelocking were achieved. Moreover we obtain very short locking times (< 3 ns) and a very stable operation at high gain currents.

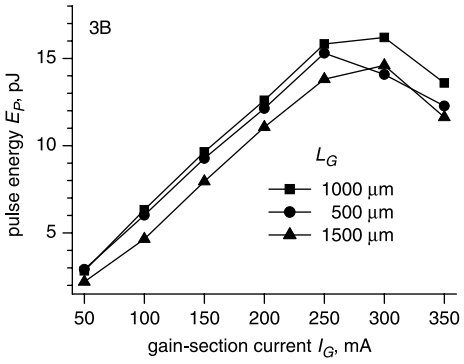

Fig. 11 *Structure 3B, pulse energy dependence on current through gain section for different lengths of this section*

Absorber section: $N_{tr} = 7.5$–$30 \times 10^{18}\,\mathrm{cm}^{-3}$. Other parameters same as Fig. 9

In Figs. 12*a*, *b*, *c* and *d* the corresponding axial distributions of the carrier density and of the right and left travelling optical power are depicted for different time points. It is assumed that the front facet with a reflectivity of $R_f = 0.05$ is located at $z = 0$. The structure is cut at $z = 3$ mm to magnify the absorber and gain sections. In the following we will describe the temporal behaviour of the different axial distributions in more detail. Figure 12*a* shows the situation before the reflected pulse arrives at the highly pumped gain section ($I_G = 300$ mA). The carrier density in the gain section has reached the maximum value. In the gain section adjacent to the absorber section amplified spontaneous emission leads to growing optical power which limits the maximal reachable carrier density in the gain section and leads to an increase of the carrier density and hence to a decrease of the absorption in the absorber section adjacent to the gain section by the interband absorption of the photons. Nevertheless, most of the absorber section is mainly non-transparent. Somewhat later (Fig. 12*b*) the pulse travels through the gain section and the peak power is

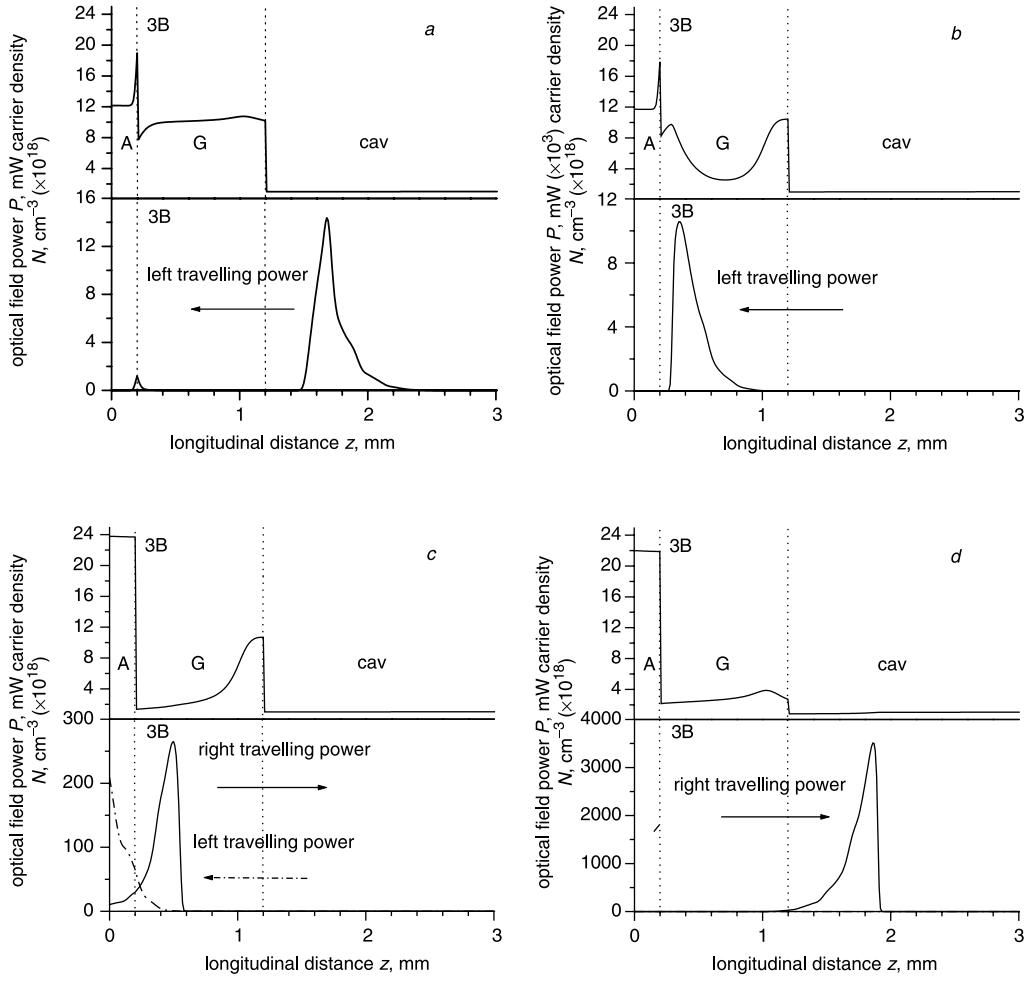

Fig. 12 *Structure 3B, axial profiles of carrier density (top) and optical power (bottom) at various times for an optimised structure*

a $t = 0\,ps$
b $t = 17.5\,ps$
c $t = 30\,ps$
d $t = 47.5\,ps$

The front facet is located at $z = 0$. The dashed vertical lines indicate boundaries of different sections. Gain-section current $I_G = 300$ mA. Other parameters same as Fig. 13

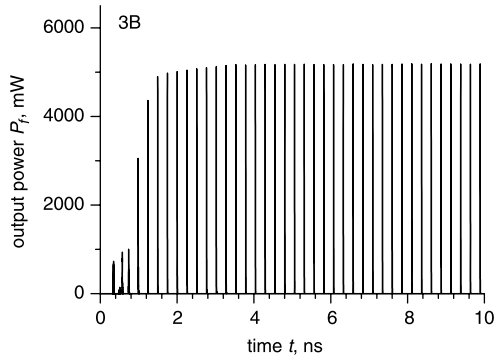

Fig. 13 *Structure 3B, start of hybrid modelocking for optimised structure for sinusoidal shaped absorber-current pulses with amplitude $\Delta I_A = 30\,mA$ and repetition frequency 3925 MHz (length 127.4 ps)*

strongly amplified. A strong spatial hole burning in the gain section can be observed which is supported by the small spatial pulse width of 200 μm. In Fig. 12*c* the amplified pulse is partially emitted, partially reflected at the front facet. The carrier density in the whole absorber section has now reached the transparency density. However, by the interband absorption of the photons excess carriers were generated firstly in the part of the absorber section adjacent to the gain section. This leads to an increase of the carrier density there and hence to a decrease of the absorption. Something like a 'transparency front' can be observed. The small part of the pulse reflected at the front facet reduces the carrier density in the gain section further owing to stimulated recombination while it is amplified, as seen in Fig. 12*d*. The carrier density in the gain section is strongly reduced towards the transparency density and the amplified reflected pulse travel along its long way to the DBR. This is an optimal operational mode.

4 Summary

We have shown by numerical simulations using the LDSL tool, that 1 cm-long monolithic multisection DBR lasers where the active layer extends over all sections can be used for the generation of modelocked pulses. The most promising configuration uses an absorber section at the front side, followed by the gain, cavity and DBR sections. The generation of short pulses (< 5 ps) with high energies (>10 pJ) and time-bandwidths products near the transform limit are realisable. It should be noted that, in this study, successful modelocking was obtained using a slow saturable absorber. An optimal length of the gain section around 10 00 μm was found. A DBR stabilises the modelocking. In general, with increasing pulse energies the pulse form became more asymmetric.

5 Acknowledgment

We are indebted to M. Radziunas (WIAS Berlin) and H.-J. Wünsche (HU Berlin) for providing the LDSL tool and interesting discussions.

6 References

1 Vasil'ev, P.P.: 'High-Power high-frequency picosecond pulse generation by passively Q-switched 1.55 μm diode lasers', *IEEE J. Quantum Electron.*, 1993, **29**, pp. 1687–1692
2 Sartorius, B., Möhrle, M., Reichenbacher, S., Preier, H., Wünsche, H.-J., and Bandelow, U.: 'Dispersive self-Q-switching in self-pulsating DFB lasers', *IEEE J. Quantum Electron.*, 1997, **33**, pp. 211–218
3 Hasler, K.-H., Wenzel, H., Klehr, A., and Erbert, G.: 'Simulation of the generation of high–power pulses in the GHz range with three-section DBR lasers', *IEE Proc., Optoelectron.*, 2002, **149**, pp. 152–160
4 Derickson, D.J., Helkey, R.J., Mar, A., Karin, J.A., Wasserbauer, J.G., and Bowers, J.E.: 'Short pulse generation using multisegment mode – locked semiconductor lasers', *IEEE J. Quantum Electron.*, 1992, **28**, pp. 2186–2202
5 Derickson, D.J., Helkey, R.J., Mar, A., Wasserbauer, J.G., and Bowers, J.E.: 'Mode – locked semiconductor lasers', *Microwave J.*, 1993, **33**, pp. 97–105
6 Kapon, E. (Ed.): 'Semiconductor lasers I: fundamentals' (Academic Press, San Diego, London, 1999), pp. 269–280
7 Avrutin, E.A., Marsh, J.H., and Portnoi, E.L.: 'Monolithic and multi-gigahertz modelocked semiconductor lasers: Constructions, experiment, models and applications', *IEE Proc. Optoelectron.*, 2000, **147**, (4), pp. 251–278
8 Kaiser, R., Hüttl, B., Heidrich, H., Fidorra, S., Rehbein, W., Stolpe, H., Ebert, W., and Sahin, G.: 'Tunable monolithic mode – locked lasers on InP with low timing jitter', *IEEE Photonics Technol. Lett.*, 2003, **15**, (5), pp. 634–636
9 Rayborn, G., Hansen, P.B., Koren, U., Miller, B., Young, M.G., Newkirk, M.A., Iannone, P.P., Burrus, C.A., Centanni, J., and Zirngibl, M.: 'Active modelocking at 4.4 GHz in a 1-cm long monolithic extended –cavity laser'. Proc. IEEE LEOS 1992 Annual Meet., 1992, Boston, MA, Paper DLTA4.3, pp.167–168
10 Hansen, P.B., Rayborn, G., Koren, U., Miller, B.I., Young, M.G., Newkirk, M.A., Chien, M.-D., Tell, B., and Burrus, C.A.: '2 cm long monolithic multisection laser for active modelocking at 2.2 GHz', *Electron. Lett.*, 1993, **29**, pp. 739–741
11 Hansen, P.B., Rayborn, G., Koren, U., Miller, B.I., Young, M.G., Chien, M.-D., Burrus, C.A., and Alferness, R.C.: '5.5 mm long InGaAsP monolithic extended - cavity laser with an integrated Bragg – reflector for active mode – locking', *IEEE Photonics Technol. Lett.*, 1992, **4**, pp. 215–217
12 Hansen, P.B., Rayborn, G., Koren, U., Iannone, P.P., Miller, B.I., Young, M.G., Newkirk, M.A., and Burrus, C.A.: 'InGaAsP monolithic extended – cavity lasers with integrated saturable absorbers for active, passive, and hybrid modelocking at 8.6 GHz', *Appl. Phys. Lett.*, 1993, **62**, pp. 1445–1447
13 Liu, H.F., Arahira, S., Kunii, T., and Ogawa, Y.: 'Generation of wavelength-tunable transform-limited pulses from a monolithic passively modelocked distributed DBR semiconductor laser', *IEEE Photonics Technol. Lett.*, 1995, **7**, pp. 1139–1141
14 Kim, D.Y., Pelusi, M.D., Ahmed, Z., Novak, D., Liu, H.F., and Ogawa, Y.: 'Ultra-stable millimetre-wave signal generation using hybrid modelocking of a monolithic DBR laser', *Electron. Lett.*, 1995, **31**, pp. 733–734
15 Khalfin, V.B., Arnold, J.M., and Marsh, J.H.: 'A theoretical model of synchronisation of a mode – locked laser with an external pulse stream', *IEEE J. Select. Top. Quantum Electron.*, 1995, **1**, pp. 523–527
16 Yang, W., and Gopinath, A.: 'Study of passive modelocking of semiconductors lasers using time – domain modelling', *Appl. Phys. Lett.*, 1993, **63**, pp. 2717–2719
17 Jones, D.J., Zhang, L.M., Caroll, J.E., and Marcenac, D.D.: 'Dynamics of monolithic passively mode – locked semiconductor lasers', *IEEE J. Quantum Electron.*, 1995, **31**, pp. 1051–1058
18 Lowery, A.J.: 'Transmission – line modelling of semiconductor lasers: the transmission line model', *Int. J. Numer. Model.*, 1990, **2**, pp. 249–265
19 Lowery, A.J., and Marshall, I.W.: 'Numerical simulations of 1.5 μm actively mode – locked semiconductor lasers including dispersive elements and chirp', *IEEE J. Quantum Electron.*, 1991, **27**, pp. 1981–1989
20 Salvatore, R., Sanders, S., Schrans, T., and Yariv, A.: 'Supermodes of high-repetition-rate passively modelocked semiconductor lasers', *IEEE J. Quantum Electron.*, 1996, **32**, (6), pp. 941–952
21 Lecce, M., and Montrosset, I.: 'Analysis of integrated mode – locked semiconductor lasers: spectral domain approach', *IEE Proc., Optoelectron.*, 2001, **148**, pp. 266–272
22 http://www.wias-berlin.de/software/ldsl/
23 Radziunas, M., Wünsche, H.-J., Sartorius, B., Brox, O., Hoffmann, D., Schneider, K.R., and Marcenac, D.: 'Modeling self-pulsating DFB lasers with an integrated phase tuning section', *IEEE J. Quantum Electron.*, 2000, **36**, pp. 1026–1034
24 Wünsche, H.-J., Bandelow, U., Wenzel, H., and Marcenac, D.D.: 'Self pulsations by mode degeneracy in two-section DFB lasers', *Proc. SPIE*, 1995, **2399**, pp. 195–206
25 Bandelow, U., Wünsche, H.-J., and Sartorius, B.: 'Dispersive self Q – switching in DFB lasers: theory versus experiment', *IEEE J. Sel. Top. Quantum Electron.*, 1997, **3**, pp. 270–278
26 Bandelow, U., Radziunas, M., Sieber, J., and Wolfrum, M.: 'Impact of gain dispersion on the spatio – temporal dynamics of multisection lasers', *IEEE J. Quantum Electron.*, 2001, **37**, pp. 183–188
27 Wünsche, H.-J., Radziunas, M., Bauer, S., Brox, O., and Sartorius, B.: 'Modeling of mode control and noise in self – pulsating phaseCOMB lasers', *IEEE J. Sel. Top. Quantum Electron.*, 2003, **9**, pp. 857–864
28 Hofmann, L., Klehr, A., Bugge, F., Wenzel, H., Smirnitski, V., Sebastian, J., and Erbert, G.: '180 mW DBR lasers with first-order gratings in GaAs emitting at 1062 nm', *Electron. Lett.*, 2000, **36**, pp. 534–535
29 Klehr, A., Bugge, F., Erbert, G., Hofmann, L., Knauer, A., Sebastian, J., Smirnitski, V.B., Wenzel, H., and Tränkle, G.: '300 GHz continuously

tunable high power three section DBR laser diode at 1060 nm', Inst. Phys. Conf. Ser., 2000, **166**, pp. 383–386
30 Klehr, A., Hasler, K.-H., Wenzel, H., and Erbert, G.: 'Generation of high-power pulses in the GHz range with three-section DBR lasers', *Proc. SPIE*, 2002, **4651**, pp. 63–72
31 Ellmers, C., Girndt, A., Hofmann, M., Knorr, A., Rühle, W.W., Jahnke, F., Koch, S.W., Hanke, C., Korte, L., and Hoyler, C.: 'Measurement and calculation of gain spectra for (GaIn)As/(AlGa)As single quantum well lasers', *Appl. Phys. Lett.*, 1998, **72**, pp. 1647–1649
32 Radziunas, M.: 'LDSL documentation', WIAS, Weierstrass Institut für angewandte Analysis und Stochastik, Berlin, Germany, 2000
33 Carroll, J.E., Whiteaway, J.E.A., and Plumb, D.: 'Distributed feedback semiconductor lasers' (IEE, London, 1998, 1st edn.)
34 Wenzel, H., Erbert, G., and Enders, P.: 'Improved theory of the refractive-index change in quantum-well lasers', *IEEE J. Select. Top. Quantum Electron.*, 1999, **5**, pp. 637–642
35 Vurgaftman, I., and Meyer, J.R.: 'Band parameters for III-V compound semiconductors and their alloys', *Appl. Phys. Rev.*, 2001, **89**, p. 5839
36 Schell, M., Weber, A., Schöll, E., and Bimberg, D.: 'Fundamental limits of sub-ps pulse generation by active modelocking of semiconductor lasers: The spectral gain width and the facet reflectivities', *IEEE J. Quantum Electron.*, 1991, **27**, (6), pp. 1661–1668
37 Buus, J.: 'Single frequency semiconductor lasers', Tutorial texts in optical engineering (SPIE, Washington, 1991), Vol. TT-5